Fully automated reconstruction of three-dimensional vascular tree structures from two orthogonal views using computational algorithms and production rules

Iching Liu
Ying Sun
University of Rhode Island
Department of Electrical Engineering
Kingston, Rhode Island 02881

Abstract. A system for reconstructing 3-D vascular structures from two orthogonally projected images is presented. The formidable problem of matching segments between two views is solved using knowledge of the epipolar constraint and the similarity of segment geometry and connectivity. The knowledge is represented in a rule-based system, which also controls the operation of several computational algorithms for tracking segments in each image, representing 2-D segments with directed graphs, and reconstructing 3-D segments from matching 2-D segment pairs. Uncertain reasoning governs the interaction between segmentation and matching; it also provides a framework for resolving the matching ambiguities in an iterative way. The system was implemented in the C language and the C Language Integrated Production System (CLIPS) expert system shell. Using video images of a tree model, the standard deviation of reconstructed centerlines was estimated to be 0.8 mm (1.7 mm) when the view direction was parallel (perpendicular) to the epipolar plane. Feasibility of clinical use was shown using x-ray angiograms of a human chest phantom. The correspondence of vessel segments between two views was accurate. Computational time for the entire reconstruction process was under 30 s on a workstation. A fully automated system for two-view reconstruction that does not require the *a priori* knowledge of vascular anatomy is demonstrated.

Subject terms: two-view reconstruction; knowledge-based approach; medical imaging; three-dimensional vascular tree; segment matching; ruled-based system; biplane angiography.

Optical Engineering 31(10), 2197–2207 (October 1992).

1 Introduction

This study is motivated by the need for determining 3-D structures of blood vessels from biplane angiograms. Angiograms are x-ray images of blood vessels enhanced by intravascular infusion of an x-ray contrast agent. A biplane angiographic system contains two pairs of x-ray tubes and image intensifiers such that two angiograms of the vasculature from different angles can be obtained almost simultaneously. Although two views of any object reveal very little about the object's 3-D structure, it is often difficult to increase the number of simultaneous angiographic views above two in clinical situations. This is because of the limited x-ray dose that a patient should receive and the constraint of space and access angle surrounding the patient, especially in an intraoperative situation. The need for reconstructing 3-D vascular structures arises from both cardiology[1] and neurology.[2] The reconstructed 3-D images would be useful for diagnosing blood vessel abnormalities and for planning surgery. Because of the pumping motion of the heart and/or the wash-out of the contrast agent, the process to be imaged is often a dynamic one. A system to image blood vessels must provide a relatively high temporal resolution. Furthermore, the width of blood vessels is generally small compared to the size of some other organs. Thus, the system must also provide a relatively high spatial resolution. Other 3-D imaging modalities usually fall short in these categories. For example, x-ray computer tomography has a temporal resolution limitation.[3] Magnetic resonance imaging has a spatial resolution limitation. Its temporal resolution also becomes limited when better image quality is preferred at the sacrifice of prolonging acquisition time.[4]

The two-view reconstruction problem is quite different from the conventional tomographic reconstruction problem in nature. There exist certain ambiguities that make the solution to the two-view reconstruction problem nonunique. Such ambiguities exist even when the object to be reconstructed is a skeletal structure without any volumetric detail.[5] Nevertheless, medical experts often manage to extract 3-D information from biplane angiograms based on their knowledge of the imaging modality, of the anatomy, and from matching local and global features between the two views. Garreau et al.[6] developed a knowledge-based approach to this problem. Models based on the coronary artery anatomy and view angles were used for 3-D reconstruction and labeling of vascular networks from biplane angiograms.

Paper 17061 received June 28, 1991; revised manuscript received April 9, 1992; accepted for publication April 9, 1992.

The following problems with the model-based approach were noted: (1) morphological changes of coronary arteries induced by patients' physiopathological states, (2) weak interaction between the high (knowledge-based) and the low (computational) level, and (3) lacking feedback from segment matching to process the original images. In this study, we propose a fully automated approach that does not rely on the *a priori* assumption of an object model. Signal-processing algorithms and artificial intelligence techniques are equally emphasized; signal-processing algorithms are essential to segmenting and representing 2-D tree structures in each view. However, incorrect segmentation is almost inevitable because of overlapping vessel segments, interference from irrelevant anatomical structures, and the presence of various types of noise in the angiograms.[7] Artificial intelligence techniques are essential to resolving the errors in segmentation and the ambiguities in matching segments between two views.

In this study, our attention is focused on the orthogonal views. When the separation angle between the view directions is 90 deg, the information about the 3-D structures is at its maximum; however, the correspondence problem is most difficult to solve. The solution for orthogonal views can be generalized for other viewing geometries including stereoscopic views and oblique views, which are obtained with more than one view-rotation axis. In this paper, first, the problem of two-view reconstruction is stated. Second, the proposed approach and the system architecture are outlined. Third, a detailed description of the various computational algorithms and the production rules is provided. Then, the system performance of reconstructing a tree model and a coronary artery phantom is presented. Finally, discussion and conclusions are given.

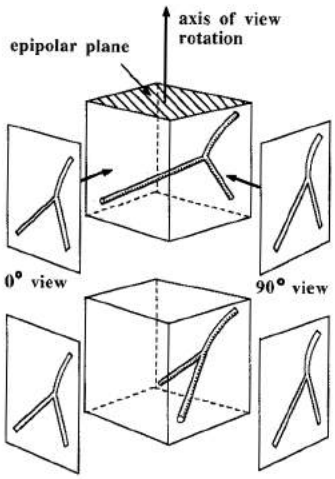

Fig. 1 Ambiguity in the two-view reconstruction problem. Two possible solutions are shown for the same given pair of orthogonal views.

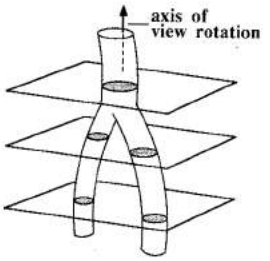

Fig. 2 With the conventional approach of tomographic reconstruction, transaxial frames are first reconstructed individually; then, the interframe continuity is explored.

2 Two-View Reconstruction Problem

We attempted to reconstruct a 3-D tree structure from two images obtained with a 90-deg separation of the view directions. The skeletal structure (centerlines) of the tree is of primary interest. The cross sections along the centerline of a segment are approximated by circular disks. The presence of ambiguities in matching segments between two views makes the two-view reconstruction problem formidable. As demonstrated by the example in Fig. 1, two possible 3-D structures for the given pairs of orthogonal views exist. This ambiguity is caused by the fact that the tree contains a node spawning off two symmetric child segments. Furthermore, the two child segments span the same range on the axis around which the view direction is rotated. Matching a segment in one view to a segment in the other view relies mainly on the epipolar constraint. The epipolar constraint forces a matching segment pair to span the same range on the view-rotation axis. Thus, the symmetric child segments in Fig. 1 cause a matching ambiguity if one relies exclusively on the epipolar constraint for clues. It can be shown that, for a binary tree containing m nodes whose subtrees are symmetric, a total of 2^m possible matchings of segments between the two views exist.[5] Nevertheless, in the case of vascular imaging, the probability of having a symmetric subtree is not likely to be high, and additional information such as the size of the vessel is often available to help resolve this type of ambiguity.

For the classic problem of tomographic reconstruction, projections from many angles around a view-rotation axis are obtained. As shown in Fig. 2, each frame perpendicular to the view-rotation axis can be uniquely reconstructed from the multiple projections. Then, the object's 3-D structure is rendered by exploring the interframe continuity along the view-rotation axis. This 3-D imaging approach is a two-step process in which 2-D slices are independently formed before the 3-D rendering. For the two-view reconstruction problem under investigation, however, the object's connectivity along the view-rotation axis provides crucial information for recognizing the segment correspondence. Thus, the process for determining segment positions on a 2-D slice (the matching problem) should not be independent of the process for exploring the object's connectivity (the tracking and segmentation problem). In our proposed approach to this problem, we emphasize (1) manipulation of directed graphs for representing segment connectivity, (2) provision for interaction between segmentation and matching, and (3) use of uncertain reasoning in dealing with matching ambiguities.

3 Proposed Solution

There are two major components in the proposed system: (1) low-level computational algorithms implemented in the C language and (2) high-level production rules implemented in the C Language Integrated Production System (CLIPS).[8]

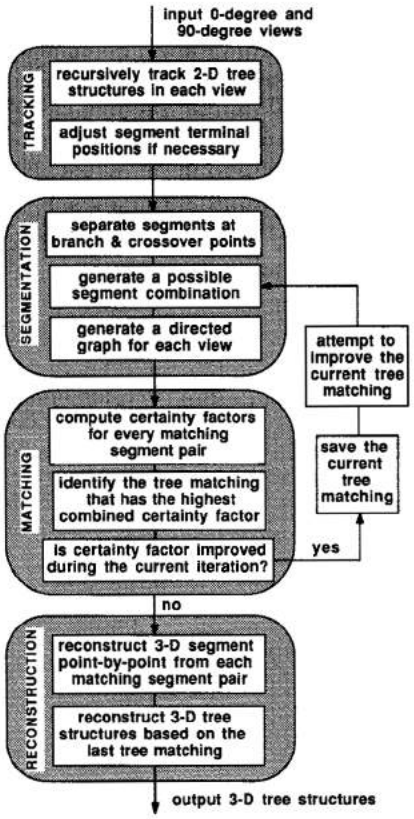

Fig. 3 Process flow diagram of the rule-based system for fully automated reconstruction of 3-D tree structures from two orthogonal views.

A global database is used to store facts about the tree structure, which are found as the tracking process proceeds. The global database also provides a common ground for communication between the computational algorithms and the production rules. Figure 3 shows the process flow diagram. In the tracking stage, the 2-D tree structure in each image is extracted by using a recursive tracking algorithm. In the segmentation stage, the 2-D tree structure is decomposed into fundamental segments. A fundamental segment is one that cannot be further decomposed. A possible combination of fundamental segments is attempted and a directed graph is formed for representing the tree connectivity. In the matching stage, domain-specific knowledge, such as the epipolar constraint and the width and connectivity of segments, is used. Certainty factors are computed to assess the goodness of a segment matching, the matching of a segment in one view to a particular segment in the other view. All certainty factors are combined for a tree matching, the collection of segment matchings for all segments in the tree structure. The certainty factors also provide clues as to where a problem exists for the current tree matching and what might improve the situation. By feeding matching difficulties back to the segment-combination stage, interaction between the segmentation in each view and the correspondence between views is allowed. The segmentation-matching iteration terminates when the total certainty factor ceases to improve. In the reconstruction stage, the tree matching that corresponds to the highest total certainty factor is used to reconstruct a 3-D tree structure.

4 Computational Algorithms

Computational algorithms perform the following tasks: (1) tracking of the tree segments in an image, (2) decomposing of the tracking result into fundamental segments, (3) generating of a direct-graph representation for the segment connectivity, (4) reconstructing the 3-D centerlines and cross sections from the matching segment pairs, and (5) projecting of the reconstructed 3-D tree model onto a given view. These algorithms are implemented in C-language procedures, which can be called on and used directly as commands in the CLIPS shell.

4.1 *Recursive Tracking of 2-D Tree Structures*

Recursive tracking is performed for each input image to obtain a 2-D structural description as detailed as possible, understanding that error in the structural description is unavoidable because of the presence of noise and overlapping segments. A previously developed tracking algorithm[9] is used to identify the 2-D tree structure starting from a given root node. The core of the algorithm is an adaptive tracking procedure that detects the centerline, lumen width, and direction of a major vessel segment. The tracking procedure sequentially detects the incremental sections along a vessel segment using an extrapolation-update scheme. The extrapolation-update process is guided by a matched filter applied to a scan line that is perpendicular to the current search direction and at a look-ahead distance away. Next, bifurcation points where side branches launch off from the major segment are detected. The tracking and branch-point detection procedures are recursively implemented for each detected branch point. To prevent repetitive tracking over the same segment, a detection-deletion scheme is employed. After a segment and all branch points on it have been identified, the segment is deleted from the image and filled with the background pixel values surrounding the segment. The result of this recursive programming is a breadth-first search that identifies the entire 2-D tree structures.[10] Each tracked segment is parameterized and stored as facts in the global database according to the following format:

```
(segment_table
   (start_point sx sy)
   (end_point ex ey)
   (start_direction sd)
   (end_direction ed)
   (average_width aw)
)
```

The point-by-point information along the entire segment is also saved in a separate data structure.

4.2 *Manipulation of Segments*

The recursive tracking delineates a 2-D tree structure in each view. However, there is usually room for improvement in this preliminary description of structure. At a crossover, where two segments appear overlapping in the image, the tracking path follows the segment that presents the strongest signal to the tracking algorithm. Thus, the segment connectivity determined by the tracking process may not reflect the actual connectivity. The direction of each incident segment at a crossover provides useful information to reveal the actual connectivity. Although the tracking algorithm

does determine the direction for every point of the segment centerline, this direction information is usually not reliable near a terminal (i.e., start, end, branch, or crossover) point. To improve the direction estimates, we perform an eigenvector fit to the first five points of a terminal. Let $(x_i, y_i), i = 1,2,\ldots,5$, be the coordinates of these five points and $(\bar{x}, \bar{y})$ be their center of mass. The covariance matrix **C** is computed according to:

$$\mathbf{C} = \begin{bmatrix} \sum_{i=1}^{5}(x_i-\bar{x})^2 & \sum_{i=1}^{5}(x_i-\bar{x})(y_i-\bar{y}) \\ \sum_{i=1}^{5}(y_i-\bar{y})(x_i-\bar{x}) & \sum_{i=1}^{5}(y_i-\bar{y})^2 \end{bmatrix} . \quad (1)$$

The best fit line goes through the center of mass, and its direction is defined by the eigenvector that corresponds[11] to the larger eigenvalue of matrix **C**.

To improve the 2-D structural description, the tracked segments are first separated into fundamental segments and then recombined at crossovers. By definition, a fundamental segment must not contain any branch or crossover point between the two terminals. An example in Fig. 4 illustrates the process of manipulating the structural description. In Fig. 4(a), a directed graph that reflects the path of recursive tracking is shown. This directed graph first goes through a separation process. The result of this process is shown in Fig. 4(b), with all start, end, crossover, and branch points treated as individual nodes. A crossover is a point in the image where two or more spatially separate segments appear overlapping. In the present analysis, we assume that a crossover node has exactly four incident segments. This restriction, however, can easily be relaxed with the expansion of the knowledge base to deal with the rarely occurring case of more than four incident segments at a crossover. The crossover node is removed by joining the appropriate pairs of fundamental segments. The pairing of segments is based on the continuation of the segments' centerlines and eigenvectors. A node with two incident segments can also occur as a result of severe stenosis or abrupt change in segment direction; the two fundamental segments are joined and the node is removed. After the process of combining segments, the final directed graph is shown in Fig. 4(c).

4.3 *Reconstruction of 3-D Tree Structures*

Once the tree matching is identified, reconstruction of the 3-D tree structure is done segment by segment. The reconstruction of each 3-D segment is accomplished using back projection on a point-by-point basis. For simplicity, we assume a parallel-beam geometry. To satisfy the epipolar constraint, a matching segment pair must span the same range on the view-rotation axis. If a minor discrepancy is observed, the terminal points are adjusted by the following rules. The terminal of one segment is extended by incorporating additional points to match up with the corresponding terminal of the opposing segment. Matching centerline points usually begins at the highest point of a centerline. This point may or may not be a terminal. Matching is done sequentially along the two centerlines and is keyed to the vertical coordinate. When the vertical coordinate of one centerline changes and the vertical coordinate of the other centerline does not follow, extra points are added. In the case where the vertical range spanned by the segment is small (less than a given threshold), the segment is considered lying in a horizontal direction. For horizontal segments, matching always begins at a terminal and proceeds sequentially along the matching centerlines. At each point of the 3-D centerline the cross section is represented by a circular disk; the radius of the circle is defined by the average of the two segment widths at the matching centerline points.

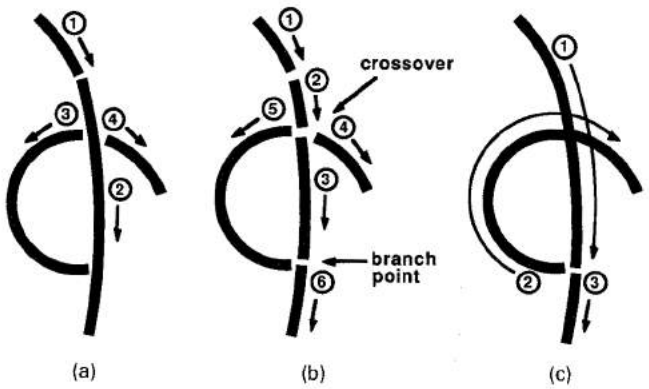

Fig. 4 Example of the directed-graph representation for a tree structure (a) delineated by the recursive tracking process, (b) after separation into fundamental segments, and (c) after combining segments at the crossover point.

5 Production Rules

The production rules are responsible for (1) directing the flow of the reconstruction process, (2) reconciling an inconsistency between the two views possibly caused by a segmentation error, (3) matching segment pairs between the two views, (4) evaluating certainty factors for matching segment pairs, and (5) generating an alternative of segment combination that may improve the total certainty factor. The production rules follow the format: IF *conditions* THEN *actions*, and are implemented in CLIPS, which has a built-in forward chaining inference engine.[8]

5.1 *Taxonomy of Rules*

The knowledge base contains 94 rules. They are summarized as follows:

- 11 control rules to direct the flow of the reconstruction process
- 2 tracking rules to initiate and terminate the tracking processes
- 14 terminal rules to adjust positions of segment terminal points and, if necessary, to combine nodes that are within a close vicinity
- 6 segmentation rules to parse the tracked tree structures into fundamental segments
- 11 combination rules to handle the problems of crossover and discontinuity, and to generate a directed-graph representation
- 19 correspondence rules to create a solution space for the correspondence problem, to initiate the computation of certainty factors, and to identify the best possible matching of segments between the two views
- 23 feedback rules to identify matching problems based

on the certainty factors and to suggest possible ways of segment combination for improving certainty

- 6 retraction rules to allow another possible segment combination by retraeting certain existing facts
- 2 reconstruction rules to initiate the 3-D reconstruction and to project the reconstructed 3-D structure onto a user-specified view plane.

5.2 *Sample Rules*

It is obviously impossible to describe every rule in detail here. However, we present two rules as examples. The rules were chosen to exemplify how the knowledge is represented and how the computational algorithms are incorporated into the rule-based system. The first sample rule is responsible for detecting two segments at a crossover. It is activated by the coexistence of the following facts: (1) a particular view is selected; (2) segment ?*v*1 has an ending point ?*p*1 and an ending direction vector ?*d*1; (3) segment ?*v*2 has the starting point ?*p*1 and a starting direction vector ?*d*2; (4) segment ?*v*3 has a starting point ?*p*3*s* and an ending point ?*p*3*e*; (5) segment ?*v*4 has a starting point ?*p*4*s* and an ending point ?*p*4*e*; (6) points ?*p*1, ?*p*3*s* (or ?*p*3*e*),and ?*p*4*s* (or ?*p*4*e*) are identical; and (7) phase difference between vectors ?*d*1 and ?*d*2 are within a range. When fired, the rule causes the action of asserting a segment combination fact. The following codes define this rule.

```
(defrule detect_combining_segments
  (which_view ?view_id)
  (segment_table (id ?v1)(end_point ?p1)(end_direction
    ?d1))
  (segment_table (id ?v2)(start_point ?p1)(start_direction
    ?d2))
  (segment_table (id ?v3)(start_point ?p3s)(end_point ?p3e))
  (segment_table (id ?v4)(start_point ?p4s)(end_point ?p4e))
  (test (or (and (= ?p1 ?p3s) (= ?p3s ?p4s))
    (and (= ?p1 ?p3e) (= ?p3e ?p4s))
    (and (= ?p1 ?p3e) (= ?p3e ?p4e))
    (and (= ?p1 ?p3s) (= ?p3s ?p4e)) ))
  (test (< abs(- ?d1 ?d2) RANGE) )
  =>
  (assert (connect_end_of_segment ?v1 to_start_
    of_segment ?v2) )
)
```

The second example is responsible for joining two segments. It is activated by the coexistence of the following facts: (1) a particular view is selected, (2) there is a call for connecting the end of segment ?*v*1 to the start of segment ?*v*2, (3) segment ?*v*1 has a complete description in the segment table, and (4) segment ?*v*2 has a complete description in the segment table. When fired, the rule causes the following action: (1) remove the call for joining these two segments; (2) delete segment ?*v*2 from the segment table; and (3) call a C subroutine to join the two segments by adjusting centerline, start/end points, and average width in the global database. The following codes define this rule.

```
(defrule join_two_segments
  (which_view ?view_id)
  ?fact1 <- (connect_end_of_segment ?v1 to_start_
    of_segment ?v2)
  (segment_table (id ?v1)(start_point ?sp)(start_direction
    ?sd))
  ?fact2 <- (segment_table (id ?v2) (end_point ?ep)
    (end_direction ?ed)(average_width ?aw))
  =>
  (retract ?fact1 ?fact2)
  (C_join_segment ?v1 ?sp ?sd ?v2 ?ep ?ed ?aw ?view_
    id)
)
```

6 Uncertainty in Segment Correspondence

Reasoning under uncertainty is an important feature of this system for solving the problem of segment correspondence. Uncertainty arises from ambiguities in matching, faults in tracking 2-D tree structures, and errors in combining fundamental segments at crossovers. Five different certainty factors are computed to quantify the goodness of each segment matching. A certainty factor (CF) takes a value between -1 and 1,where CF $=1$ means absolutely positive, CF $=-1$ means absolutely negative, and CF $=0$ means totally uncertain. For matching segment i in one view to segment j in the other view, $\mathrm{CF}_k(i,j)$, $k=1,2,\ldots,5$, are used to assess the goodness of matching in five different categories. These categories are the parent segments' relation, the number of segments in subtree, the depth on the directed graph, the average segment width (aw), and the overlapping range on the vertical (view-rotation) axis.

6.1 *Certainty Factors*

We determine $\mathrm{CF}_1(i,j)$ by whether the parent of segment i matches the parent of segment j:

$$\mathrm{CF}_1(i,j)=\begin{cases}1, & \text{if their parents match}\\ 0, & \text{otherwise}\end{cases}. \tag{2}$$

We determine $\mathrm{CF}_2(i,j)$ by how well the total number of segments in subtree (ns) of segment i compares with that of segment j:

$$\mathrm{CF}_2(i,j)=1-2\times\frac{|\mathrm{ns}_i-\mathrm{ns}_j|}{\mathrm{maximum}(\mathrm{ns}_i,\mathrm{ns}_j)}. \tag{3}$$

We determine $\mathrm{CF}_3(i,j)$ by whether segment i and segment j are at the same depth (dp) from the root node on their directed graphs:

$$\mathrm{CF}_3(i,j)=1-2\times\frac{|\mathrm{dp}_i-\mathrm{dp}_j|}{\mathrm{maximum}(\mathrm{dp}_i,\mathrm{dp}_j)}. \tag{4}$$

We determine $\mathrm{CF}_4(i,j)$ by how well the average width (aw) of segment i matches that of segment j:

$$\mathrm{CF}_4(i,j)=2\times\frac{\mathrm{minimum}\ (\mathrm{aw}_i,\mathrm{aw}_j)}{\mathrm{maximum}(\mathrm{aw}_i,\mathrm{aw}_j)}-1. \tag{5}$$

We determine $\mathrm{CF}_5(i,j)$ by how well the range on the vertical axis spanned by segment i matches that spanned by segment j:

$$\mathrm{CF}_5(i,j)=2\times\frac{l_\cap(i,j)}{l_\cup(i,j)}-1, \tag{6}$$

where $l_{\cap}(i,j)$ is the length of the overlapping portion of segment i and segment j as projected onto the vertical axis, and $l_{\cup}(i,j)$ is the length of the total range spanned by segment i and segment j on the vertical axis. A prerequisite for accepting the matching of a particular segment pair is that CF_5 must be greater than zero. In other words, a possible tree matching will be immediately discarded if it contains a matching segment pair that has an overlapping length less than 50% of their total span on the vertical axis. This constraint effectively reduces the search space.

6.2 *Combining of Certainty Factors*

Certainty factors are combined at two levels. First, for each segment matching the five certainty factors (CF_1, CF_2, ..., CF_5) are combined into one, denoted by CF_{seg}. Second, for the entire tree matching all CF_{seg}'s are further combined into a total certainty factor, denoted by CF_{tree}, which is associated with the goodness of the tree matching. Let CF_a and CF_b denote two certainty factors to be combined, and let CF_c denote the resulting certainty factor. The following formulas govern the combining of two certainty factors:[8]

$$CF_c = \begin{cases} CF_a + CF_b - CF_a \times CF_b, & \text{if } CF_a > 0,\ CF_b > 0 \\ CF_a + CF_b + CF_a \times CF_b, & \text{if } CF_a \leq 0,\ CF_b \leq 0 \\ \dfrac{CF_a + CF_b}{1 - \min(|CF_a|, |CF_b|)}, & \text{otherwise} \end{cases} \quad (7)$$

These formulas have the properties of associativity and commutativity. Thus, they can be applied for combining multiple certainty factors. No matter what order is chosen for combining the pairs, the final result is always the same.

6.3 *Segmentation-Matching Interaction*

Another important feature of this system is an incremental approach to the solution of segment correspondence. This is accomplished by feeding the higher-level matching result back to the lower-level segmentation. First, the problematic pair of segment matching is identified. Then, the related fundamental segments are recombined and the modification is incorporated into the current tree matching for another evaluation. The rationale behind this approach is that matching of major segments is usually obvious and of high certainty. It is the side branches and overlapping branches that frequently cause matching difficulties. Thus, it makes sense to keep the highly certain matching pairs and only change the highly uncertain matching pairs. At present, matching problems are fed back to the segment combining stage, but not the recursive tracking stage. Nevertheless, even with this provision, a large class of matching problems can be solved. A matching problem is often caused by incorrectly separating and combining segments at crossovers, branch points, and stenotic sections, and only occasionally by incomplete or inconsistent tracking between the two views. Iteration is implemented to allow feedback from the matching stage to the segmentation stage. Certainty factors serve two purposes in this feedback loop: (1) to provide information about which segment pair and which of the five categories cause uncertainty in the tree matching and (2) to signal when the iteration should stop.

At present, 23 rules are implemented for the provision of feedback. The rules are activated on $CF_1 = 0$ (parent segments do not match), negative CF_2 (numbers of subtree segments are not the same), or negative CF_3 (they are not at the same depth on the directed graph). The remedial action is (1) to undo the current segment matching, (2) to combine the fundamental segment in question either with its parent segment or with its subtree, and (3) to rematch the resulting segments. The stopping criterion of the iteration is either all certainty factors are greater than zero or CF_{tree} is not improved after a recombination of segments.

7 Results

The system software was implemented on a Sun 4/490 system (Sun Microsystem, San Jose, Calif.). The verification and validation of the software were done in two parts. First, digitized video images of a tree model were used. The tree model was intentionally formed to result in overlapping segments from several view directions so that the system's capability of combining and matching segments at crossover points could be evaluated. Second, x-ray angiograms of a chest phantom were used to evaluate the system's applicability to clinical situations.

The computational time obviously depends on the complexity of the tree. In all cases described in the following, the total computational time for tracking, segmentation, matching, and reconstruction was under 30 s on the Sun 4/490 system.

7.1 *Video Images of a Tree Model*

Two mutually orthogonal images of the tree model were input to the system. The orthogonal pair was obtained with a video camera, before and after rotating the tree model by 90 deg around the vertical axis. Each image was digitized to $256 \times 256 \times 8$ bits. Figure 5 shows one example of the 0-deg view and the 90-deg view. The centerline structures identified by the tracking algorithm are shown by white pixels and superimposed with the original images for comparison. After the segment combination and correspondence, a 3-D tree structure was produced. To verify the reconstruction, the reconstructed 3-D structure was viewed from three directions which were different from the original directions (i.e., 0 and 90 deg on the epipolar plane). The view directions we chose were (1) from 45 deg (2) from -45 deg, and (3) from the bottom; the first two directions are parallel to the epipolar plane and the last is perpendicular to the epipolar plane. A ray-tracing program was used to give a 3-D perception for each reconstructed image. In Fig. 6, the actual images of the tree model at the aforementioned view directions are shown at the top and the corresponding reconstructed images are shown at the bottom. The result indicated that the relative positions of segments in the tree were accurately reflected in the reconstructed images. Thus, the segment correspondence was correctly identified by the rule-based system.

To evaluate the reproducibility of the system, the above test was repeated three times; each time a different pair of orthogonal images was used as the input. These results are shown in Fig. 7. The three columns of images in Fig. 7 correspond to the three different tests performed. For each test, five views from different directions are shown. In each view, the reconstructed centerlines (white) are overlapped with the actual image taken from the same view direction. The 0- and 90-deg images were used as the input; they

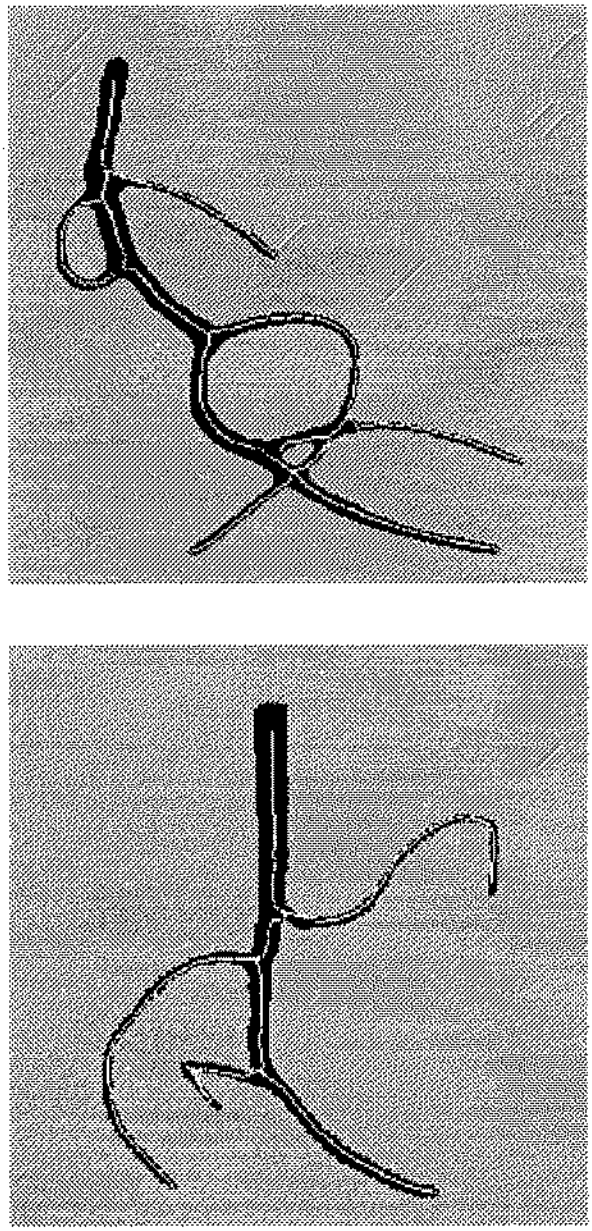

Fig. 5 Orthogonal images of a vascular model: (top) the 0-deg view, taken at an arbitrary angle and (bottom) the 90-deg view. Each image is digitized to $256 \times 256 \times 8$ bits.

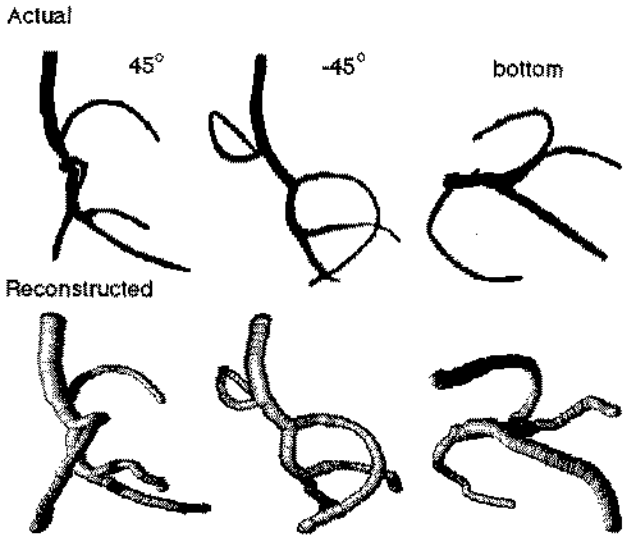

Fig. 6 Comparison between the actual views (top row) and the reconstructed views (bottom row) at the 45-deg angle on the epipolar plane (left), at the −45-deg angle on the epipolar plane (middle), and from the bottom (right).

naturally showed the smallest deviation between actual and reconstructed images. The largest deviation was always found in the bottom view. Because the bottom view pointed to a direction perpendicular to the epipolar plane, it received the least amount of 3-D information from the original input images. To characterize these deviations quantitatively, a skeletal structure was obtained from each actual image using a thinning algorithm.[12] The distance between a reconstructed centerline point and the nearest point of the skeletal structure in the actual image was determined for every point along the reconstructed centerlines. The (unbiased) standard deviation of this distance for the entire tree structure was computed. These standard deviations were further averaged across the three tests for each view direction. In Table 1, these standard deviations are shown in terms of pixels and also converted to millimeters based on the spatial resolution of 0.3 mm/pixel. Also shown are the maximum deviations, each averaged across the three tests for the given view direction. There is an intrinsic deviation of 0.9 pixel (0.27 mm) between the centerlines determined by our tracking algorithm and those determined by the thinning algorithm.

7.2 *Angiograms of a Coronary Artery Phantom*

To evaluate how the system performs on realistic vascular images, angiograms of a human chest phantom (Humanoid Systems, Carson, Calif.) were acquired using a single-plane digital angiographic system (Unicath C, Angiographic Devices Corporation, Littleton, Mass.). Angiograms were acquired from five different directions based on the viewing geometry shown in Fig. 8. The chest phantom contained a model of the human left coronary artery including both the left anterior descending branch and the circumflex branch. Figure 9 shows the cranial 45-deg view and the left lateral view, which were used as the orthogonal pair of input images. The tracked vessel centerlines are superimposed. In Fig. 10, the reconstrueted images are compared with the aetual images at the three view directions, which are lying on the caudal 45 deg plane. The results show that the relative positions of the vessel segments are correctly represented hy the reconstructed structure.

8 Discussion

In summary, a fully automated system for reconstructing 3-D vascular structures from two orthogonal views was developed. Computational algorithms were implemented to segment the 2-D structure, to produce a directed-graph representation, and to reconstruct the 3-D tree structure from matching segment pairs. Production rules were implemented to coordinate the computational algorithms, to resolve inconsistency between the views, and to identify the most probable correspondence of segments. The validity of the system was tested with video images of a tree model and

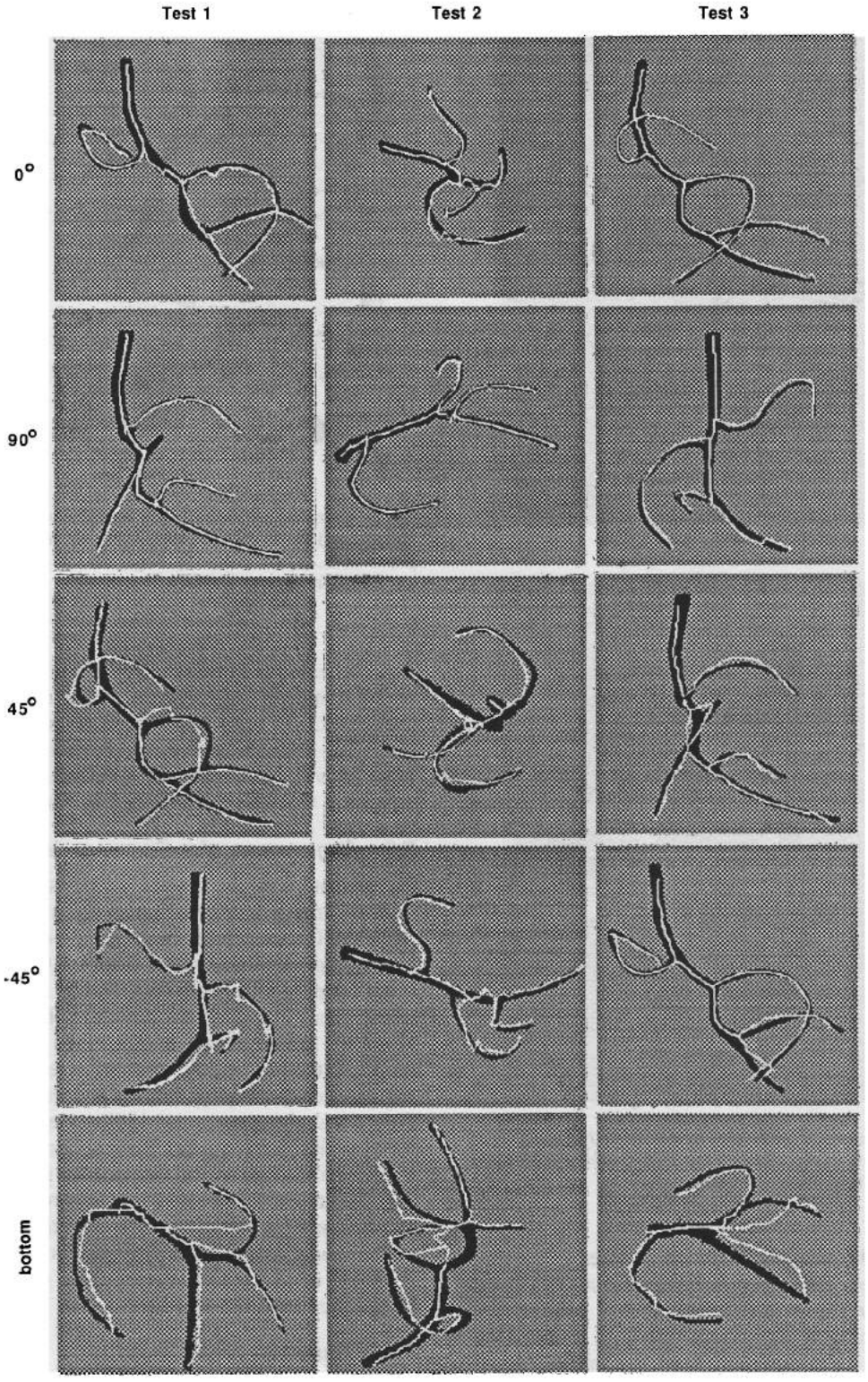

Fig. 7 In three separate tests (left, middle, and right) the reconstructed centerlines shown in white are projected and overlapped with the actual view of the tree model at each corresponding angle.

angiograms of a human chest phantom. The system showed a satisfactory performance; the correspondence of the major segments identified by the vessel-tracking algorithm was correctly determined in all cases. The standard deviation of the reconstructed centerlines was estimated to be 0.8 mm (1.7 mm) for a view direction parallel (perpendicular) to the epipolar plane. The total processing time was under 30 s on a workstation. Compared to other similar knowledge-based approaches,[13–15] the following features make our system unique. (1) There is a high degree of interaction between the high-level knowledge-based reasoning and the low-level image processing; production rules and compu-

Table 1 Standard and maximum deviations of reconstructed centerline positions for 0.3 mm/pixel spatial resolution.

	0°	90°	45°	-45°	bottom
S.D. (pixels/mm)	1.1 / 0.34	1.3 / 0.39	2.8 / 0.83	2.8 / 0.84	5.6 / 1.67
Maximum (pixels/mm)	4.1 / 1.2	4.7 / 1.4	9.7 / 2.9	9.5 / 2.8	23.5 / 7.1

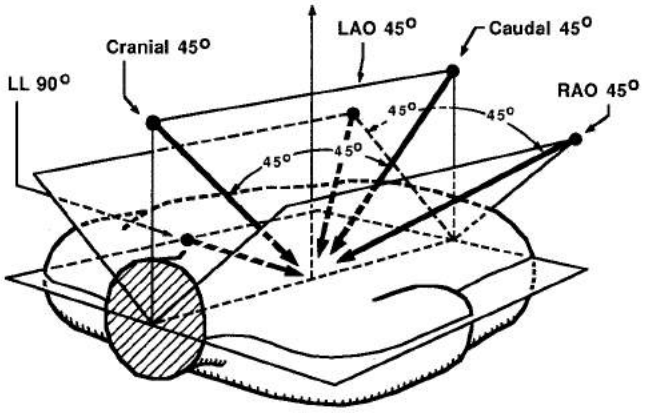

Fig. 8 Geometry for imaging the human chest phantom. Five angiograms were taken: cranial 45 deg, left lateral (LL) 90 deg, caudal 45 deg with no rotation, caudal 45 deg with a left 45 deg rotation (LAO 45 deg), and caudal 45 deg with a right 45 deg rotation (RAO 45 deg).

tational algorithms are integrated in a single software system. (2) Feedback from matching to segmentation is provided whereby the solution to segment correspondence is incrementally improved. (3) Reasoning with uncertainty is employed to deal with the fuzziness in matching segments; certainty factors are used to diagnose and remedy the matching difficulties. (4) The system does not rely on the *a priori* assumption of the vascular anatomy and specific view directions.

The segment correspondence is our main concern because an incorrect matching of segments would cause a completely erroneous reconstruction. The results in Figs. 6 and 10 show that the system successfully resolves the segment correspondence problem. A minor degree of discrepancy between the reconstructed structure and the actual structure exists. As shown in Fig. 7, the reconstructed positions of the terminals of a segment are usually accurate because several rules have been implemented to ensure the matching of terminals and to adjust the terminal's positions if necessary. However, the portion of centerline between terminals sometimes shows a higher degree of deviation. This deviation is caused by mismatch of points along the centerline. A mismatch of centerline points can arise from the following sources of error. First, because no precision mechanical device was used to rotate the tree model during image acquisition and no spatial calibration for the imaging chain was done, a certain degree of shift, tilt, and/or spatial distortion in the original input images probably existed. Second, when the direction of a segment was almost perpendicular to the view-rotation axis, very little epipolar information was available to guide the point-by-point matching. Third, although the assumption of parallel-beam geometry was accurate for video images, the x-ray angiography system used in this study had a cone-beam geometry with a 10-deg angle. The incorrect assumption of parallel beams did not cause any problem in segment matching. However, we estimated that the position deviation arising from a depth difference of 10 mm is zero at the center and 0.9 mm ($10 \times \tan 5$ deg mm) at the margin of the image because of this incorrect assumption of parallel beams. Future directions for improving the estimation of centerline position include consideration of the small-angle cone-beam geometry and development of an appropriate interpolation

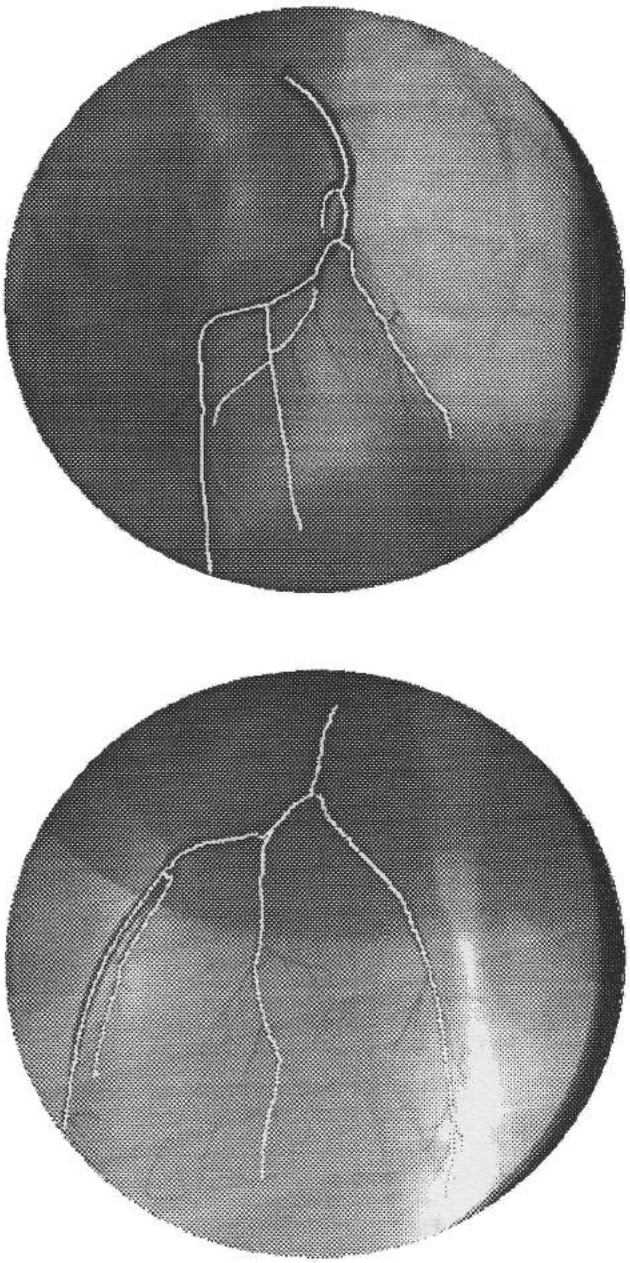

Fig. 9 Two orthogonal angiograms used as input to the reconstruction system: (top) the cranial 45-deg view and (right) the left lateral 90-deg view. Each image is digitized to $512 \times 512 \times 8$ bits.

The inclusion of anatomical knowledge would require information about the specific portion of the human body to be imaged and the specific view angles. As a consequence, the application of such systems is likely to be quite limited. Moreover, patients often do not show normal anatomy. For example, with the presence of coronary artery stenosis, the development of collaterals is usually extensive and the tortuousity of the coronary arteries can also be significantly affected. In such a case, anatomical knowledge may even become misleading. Second, we emphasize both the AI techniques and the signal processing algorithms. For certain "low-level" tasks, such as delineating the 2-D vascular structure, it is probably more suitable and definitely more efficient to use signal processing techniques instead of AI techniques. Angiograms are, in general, noisy; it is certainly more appropriate to filter out the noise than to reason out the noise. On the other hand, the ambiguities in the two-view reconstruction problem can only be resolved with some "high-level" reasoning process. In this study, a major effort has been made to ensure balance and a tight interface between signal-processing algorithms and AI techniques.

This study has demonstrated that the two-view reconstruction problem can be solved in an automated way using computational algorithms under the control of a knowledge base. The knowledge base comprises a relatively small set of production rules, and the execution of the system software is relatively fast. Using x-ray angiograms of a human chest phantom the feasibility of applying this system to a clinical environment is demonstrated. The next phase of this project should involve clinical implementation and the evaluation of efficacy of the 3-D vascular analysis. For this purpose, the ideal platform for implementing the proposed approach is a fully digital biplane angiographic system.

Acknowledgments

This work was supported by the National Science Foundation under Grant No. BCS-8910188. The authors would like to thank Norman Jolicoeur of Angiographic Devices Corporation and James Coffin of XRE Corporation for their assistance in acquiring the phantom angiograms.

References

1. B. G. Brown, E. L. Bolson, and H. T. Dodge, "Quantitative computer techniques for analyzing coronary arteriograms," *Prog. Cardiovasc. Dis.* **28**(6), 403–418 (1986).
2. C. Smets, D. Vandermeulen, P. Suetens, and A. Oosterlinck, "A knowledge-based system for the 3-D reconstruction and representation of the cerebral blood vessels from a pair of stereoscopic angiograms," in *Medical Imaging III: Image Processing, Proc. SPIE* **1092**, 130–138 (1989).
3. Y. Masuda, H. Yoshida, N. Morooka, O. Takahashi, S. Watanabe, Y. Inagaki, G. Uchiyama, and Y. Tateno, "ECG synchronized computed tomography in clinical evaluation of total regional cardiac motion: comparison of postmyocardial infarction to normal hearts by rapid sequential imaging," *Am. Heart J.* **103**(2), 230–238 (1982).
4. C. B. Higgins and M. McNamara, "Magnetic resonance imaging of ischemic heart disease," *Prog. Cardiovasc. Dis.* **28**(4), 257–266 (1986).
5. Y. Sun and E. Bergerson, "Automated 3-D reconstruction of tree-like structures from two orthogonal views," in *Proc. IEEE Int. Conf. Acoust., Speech, Signal Processing*, pp. 1296–1299 (1988).
6. M. Garreau, J. L. Coatrieux, R. Collorec, and C. Chardenon, "A knowledge-based approach for 3-D reconstruction and labeling of vascular networks from biplane angiographic projections," *IEEE Trans. Med. Imaging* **10**(2), 122–131 (1991).
7. D. P. Kottke and Y. Sun, "Segmentation of coronary arteriograms by iterative ternary classification," *IEEE Trans. Biomed. Eng.* **37**(8), 778–785 (1990).
8. J. Giarratano and G. Riley, *Expert Systems: Principles and Programming*, PWS-Kent Publishing, Boston, Mass. (1989).
9. Y. Sun, "Automated identification of vessel contours in coronary arteriograms by an adaptive tracking algorithm," *IEEE Trans. Med. Imaging* **8**(1), 78–88 (1989).
10. I. Liu and Y. Sun, "Recursive tracking of vascular trees in angiograms using a detection-deletion scheme," in *Proc. 12th Ann. Int. Conf. IEEE Eng. Med. Biol. Society*, pp. 169–170 (1990).
11. R. C. Gonzalez and P. Wintz, *Digital Image Processing*, 2nd ed., Addison-Wesley Publishing, Reading, Mass. (1987).
12. T. Y. Zhang and C. Y. Suen, "A fast parallel algorithm for thinning digital patterns," *Comm. ACM* **27**(3), 236–239 (1984).
13. G. Coppini, M. Demi, R. Mennini, and G. Valli, "Three-dimensional knowledge driven reconstruction of coronary trees," *Med. Biol. Eng. Comput.* **29**, 535–542 (1991).
14. D. Delaere, L. Maes, C. Smets, P. Suetens, A. Oosterlinck, and F. Van de Werf, "A knowledge-based system for the fully automated quantification of coronary stenotic lesions from two angiographic projections," in *Medical Imaging IV: Image Processing, Proc. SPIE* **1233**, 250–256 (1990).
15. K. Barth, B. Eicker, and J. Seissl, "Automated biplane vessel recognition in digital coronary angiograms," in *Medical Imaging IV: Image Processing, Proc. SPIE* **1233**, 266–275 (1990).
16. K. R. Hoffmann, K. Doi, H. Chan, and M. Takamiya, "Three dimensional reproduction of coronary artery trees using the double-square-box method of tracking," in *Medical Imaging II, Proc. SPIE* **914**, 375–378 (1988).
17. D. L. Parker, D. L. Pope, R. van Bree, and H. W. Marshall, "Three-dimensional reconstruction of moving arterial beds from digital subtraction angiography," *Comput. Biomed. Res.* **20**, 166–185 (1987).
18. K. Kitamura, J. M. Tobis, and J. Sklansky, "Estimating the 3-D skeletons and transverse areas of coronary arteries from biplane angiograms," *IEEE Trans. Med. Imaging* **7**(3), 173–187 (1988).
19. J. W. Peifer, N. F. Ezquerra, C. D. Cooke, R. Mullick, L. Klein, M. E. Hyche, and E. V. Garcia, "Visualization of multimodality cardiac imagery," *IEEE Trans. Biomed. Eng.* **37**(8), 744–756 (1990).
20. H. C. Kim, B. G. Min, T. S. Lee, S. J. Lee, C. W. Lee, J. H. Park, and M. C. Han, "Three dimensional digital subtraction angiography," *IEEE Trans. Med. Imaging* **1**(2), 152–158 (1982).
21. T. Saito, M. Misaki, K. Shirato, and T. Takishima, "Three-dimensional quantitative coronary angiography," *IEEE Trans. Biomed. Eng.* **37**(8), 768–777 (1990).
22. J. J. Gerbrands, J. H. C. Reiber, B. Scholts, G. Langhout, and C. J. Kooijman, "Structural analysis of the coronary arterial tree," in *Proc. IEEE Medical Imaging Image Interpretation Conf.*, pp. 54–58 (1982).
23. Y. Sun, "Knowledge-based segmentation and correspondence of vascular structures from biplane angiograms," in *Medical Imaging IV: Image Processing, Proc. SPIE* **1233**, 257–265 (1990).
24. S. A. Stansfield, "ANGY: A rule-based expert system for automatic segmentation of coronary vessels from digital subtraction angiogram," *IEEE Trans. Pattern Anal. Mach. Intell.* **8**(2), 188–199 (1986).

Iching Liu received the BS degree from National Chiao-Tung University, Hsien-Chu, Taiwan, in 1984 and the MS degree from University of Massachusetts, Lowell, Massachusetts, in 1989, both in electrical engineering. Since 1989, he has been admitted to the PhD program at the Department of Electrical Engineering, University of Rhode Island, where he has worked as research assistant and computer system administrator. Liu's PhD thesis concerns the reconstruction of 3-D blood vessel images from very limited views. His research interest includes image processing, pattern recognition, computer vision, and artificial intelligence.

Ying Sun received the BS degree from the National Taiwan University in 1978, the MS degree from the University of Rhode Island in 1982, and the PhD degree from the Worcester Polytechnic Institute in 1985, all in electrical engineering. In 1985, he joined the Department of Electrical Engineering at the University of Rhode Island as an assistant professor, and has been an associate professor since 1990. His research in medical imaging, computer-based instrumentation, and modeling of the cardiovascular dynamics has been supported by industry and the National Science Foundation. Sun has also served as a consultant to the medical device industry and medical research centers.